This is an open access article published under a Creative Commons Attribution (CC-BY) License, which permits unrestricted use, distribution and reproduction in any medium, provided the author and source are cited.

LANGMUIR

Article

pubs.acs.org/Langmuir

Molecular Dynamics Studies of Overbased Detergents on a Water Surface

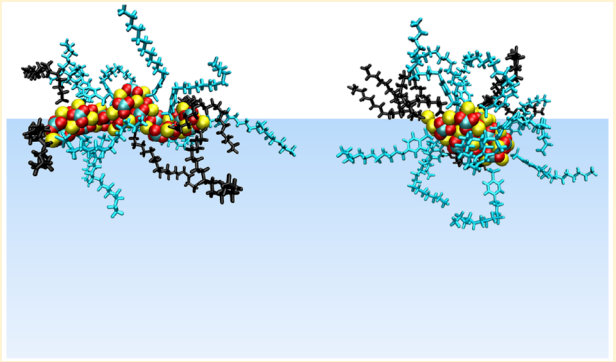
M. S. Bodnarchuk, D. Dini, and D. M. Heyes*

Department of Mechanical Engineering, Imperial College London, Exhibition Road, London SW7 2AZ, United Kingdom

A. Breakspear and S. Chahine

BP Technology Centre, Whitchurch Hill, Pangbourne RG8 7QR, United Kingdom

ABSTRACT: Molecular dynamics (MD) simulations are reported of model overbased detergent nanoparticles on a model water surface which mimic their behavior on a Langmuir trough or large water droplet in engine oil. The simulations predict that the structure of the nanoparticle on a water surface is different to when it is immersed in a bulk hydrophobic solvent. The surfactant tails are partly directed out of the water, while the carbonate core maximizes its extent of contact with the water. Umbrella sampling calculations of the potential of mean force between two particles showed that they are associated with varying degrees with a maximum binding free energy of ca. 10 k_BT for the salicylate stabilized particle, ca. 8 k_BT for a sulfurized alkyl phenate stabilized particle, and ca. 5 k_BT for a sulfonate stabilized particle. The differences in the strength of attraction depend on the proximity of nearest approach and the energy penalty associated with the disruption of the hydration shell of water molecules around the calcium carbonate core when the two particles approach. This is greatest for the sulfonate particle, which partially loses the surfactant ions to the solution, and least for the salicylate, which forms the weakest water "cage". The particles are separated by a water hydration layer, even at the point of closest approach.



I. INTRODUCTION

Hydrophobically stabilized calcium carbonate based nanoparticles are added to engine oils to neutralize strong acids such as sulfuric and nitric acid which are produced during fuel combustion. These are known as "overbased" (OB) particles because they contain more calcium (and hence calcium carbonate) than is stoichiometrically required to compensate for the charge on the surfactant ions in the system. They form classical inverse micelle structures, which enable them to be soluble in hydrophobic oil. The residual surfactant after neutralization solubilizes the polar material resulting from the engine operation and thereby reduces sludge formation. The acid neutralizing capability of the particles is measured in terms of the total base number (TBN) which is the equivalent neutralizing ability in units of milligrams of KOH per gram. Phenate, sulfonate, salicylate, and calixarate surfactants are used, and the TBN values of these particles with stearate cosurfactant in commercial OB products are typically in the range 300−400. The nanoparticles in experiment have approximately the same number of $CaCO_3$ ion pairs in the core or TBN number. A schematic diagram of the generic structure of an OB particle is given in Figure 1.

There is a body of evidence to support the nanoparticle nature of the overbased chemical additive, in which the individual particles are in the form of reverse micelles each just a few nanometers across. This comes from neutron scattering,[1−4] transmission electron microscopy (TEM),[5−9] molecular simulation,[10−19] and Langmuir trough measurements.[11,14,20] The nanoparticle composition of the product facilitates its uniform distribution on dissolution in the oil. The rate of acid neutralization can as a result be controlled more systematically by adjusting the chemistry. Extended X-ray absorption fine structure (EXAFS) microscopy shows that the central core is in the form of amorphous calcium carbonate.[21] The next region outward is formed from the polar heads of the surfactant, the cosurfactant molecules, and any residual polar solvent molecules left over from the synthesis process. The third and outermost region consists of the surfactant and cosurfactant alkyl tails. It is this region that interacts with and makes the nanoparticle soluble in the engine oil. Typical synthetic procedures and characterization of the overbased product are described in refs 22 and 23.

For this work we return to the Langmuir trough (LT) measurements, which have been used extensively to obtain the

Received: March 17, 2017
Revised: June 29, 2017
Published: June 30, 2017

 © 2017 American Chemical Society

DOI: 10.1021/acs.langmuir.7b00827
Langmuir 2017, 33, 7263−7270

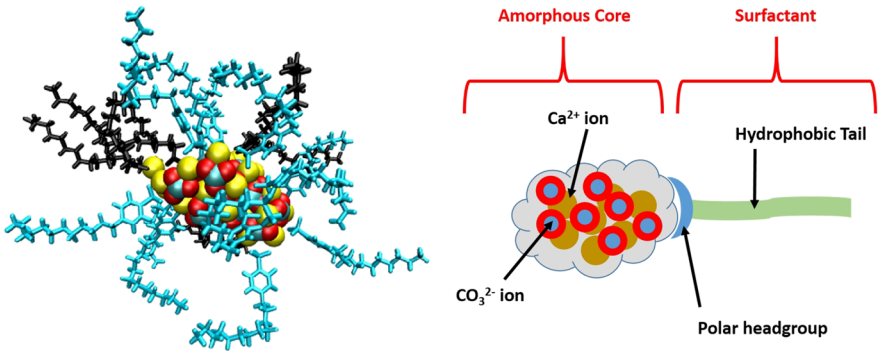


Figure 1. Schematic diagram illustrating an OB particle (left) and the different regions in a typical OB particle (right).

particle sizes and other characteristics of the overbased particle, such as the effective interaction force as a function of pair separation.[11,14,20] These are derived from a surface pressure against coverage density plot using simple trigonometry-based assumptions.[11,14,20] For example, the particles are typically assumed to be arranged in a hexagonal lattice on the air−water surface.

In this study we obtain an improved understanding and characterization of the arrangement and interaction of the nanoparticles on the water surface using molecular simulations. The particles might be considered to be structurally somewhat different on a water−air surface than in bulk oil because their environment is chemically different. Molecular simulation is ideally suited to explore these features, as currently experimental studies involving the basic Langmuir trough design do not achieve this level of atomic detail. Large-scale molecular dynamics (MD) simulations are used to explore how the structures of the overbased particles on the surface differ from their form in the bulk oil. Currently the implicit assumption is that their structure is not significantly different on the water surface compared to in a bulk hydrophobic solvent; e.g., the particles are on average spherically symmetric, for the sulfonates at least. Resolution of this issue reduces to identifying the role that the water interface plays in determining the OB particle shape and also on the effective interaction energy as a function of separation between two OB particles. Our more recent molecular simulation studies have shown that even trace amounts of water interact strongly with the OB calcium carbonate core in the bulk oil.[18,19] Therefore, it might reasonably be expected that the effects of surrounding water in the LT experiment arrangement could be significant, although this issue has yet to be fully resolved. This is one of the objectives of this study.

II. VIRTUAL EXPERIMENT METHODOLOGY

Three surfactant types were used in this study, which are a sulfurized alkylphenol (SAP), an alkyl sulfonate, and an alkyl salicylate. Three different types of simulations were performed. The first set, which are simulations A to C in Table 1, followed the process of a single nanoparticle adsorbing on a planar water surface. The second set (simulations D to F in Table 1) mimicked the adsorption of a second OB particle onto the same water layer face. The simulations were carried out at a temperature (T) of 523 K, the approximate temperature of automotive engine oil under steady running conditions long after startup. The pressure was set to 10 bar using the Parrinello−Rahman method,[24] which is the approximate pressure of the engine oil during engine operation.

Table 1. Summary of the Number of Each Species Used in the Simulations and the Identifying Code Letter

system (run code)	surfactant	H_2O	Ca^{2+}	CO_3^{2-}
SAP (A)	6	7161	16	10
sulfonate (B)	12	7161	16	10
salicylate (C)	12	7161	16	10
SAP (D)	12	16484	32	20
sulfonate (E)	24	15083	32	20
salicylate (F)	24	16494	32	20

In the third stage, steered MD and umbrella sampling was used to calculate the free energy of association between two nanoparticles of the same surfactant type, using the same number of species in the OB particle and water as in simulations D to F. The number of each species in the simulations is given in Table 1. The model nanoparticles in the simulations were performed using the Coulombic annealing and re-forming procedure invented and described in refs 17−19.

The simulations were performed using the molecular dynamics (MD) simulation code GROMACS v4.5.5.[25,26] The force field parameters were the same as those reported in refs 25 and 26. The particle mesh Ewald method[27] was used to compute the electrostatic terms in the potential, with interactions between atoms within 1.0 nm evaluated every time step and every five time steps for atom pairs further apart. Nonbonded van der Waals terms were treated using the Lennard-Jones pair potential with a cutoff of 1.2 nm. Verlet's leapfrog equation of motion integrator was used with a time step of 2 fs. The bond distances and angles of water molecules were constrained using the SETTLE algorithm,[28] and all other bonds were constrained using LINCS.[29] Temperature was regulated using a velocity rescaling thermostat with a coupling time of 0.1 ps.[30−32]

III. RESULTS AND DISCUSSION

A. Surface Preparation. In order to mimic the behavior of an OB on a water surface, a simulation box containing only water molecules in the form of a slab layer was constructed and equilibrated. A typical snapshot of the water layer is shown in Figure 2. The water plane is in the plane bounded by the cell side lengths in the x- and y-directions, and the z-direction is perpendicular to the plane of the water surface. A water layer, measuring $6 \times 8 \times 6$ nm^3, was initially formed and equilibrated for a time of 1 ns using MD in the NPT ensemble. The simulation box was then extended by 6 nm in the $+z$ and $-z$ directions, the extra space being filled with a vacuum. In all of

DOI: 10.1021/acs.langmuir.7b00827
Langmuir 2017, 33, 7263−7270

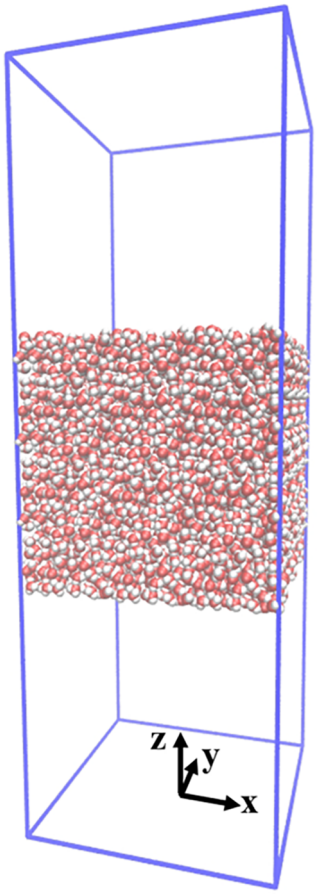


Figure 2. Representative unit cell for the OB on water surface simulations. The figure shows the water film before the OB particles were added. The periodic cell sidelength vectors make the *x*- and *y*-directions, and *z* is perpendicular to the water surface.

the subsequent simulations, a weak harmonic restraint of 5 kJ mol^{-1} nm^{-2} was applied to each oxygen atom in the water layer to reduce evaporation into the vacuum and suppress long-range transverse oscillations of the water layer. This was to mimic better the conditions in a real experiment where there is only one water surface, above a macroscopic amount of bulk water. A weak harmonic restraint was only applied in the *z*-direction, which allowed the water molecules to move freely along the water surface but not to evaporate into the vacuum. The value of the restraint was chosen to allow the layer to relax as molecules moved in the *x*- and *y*-directions but at the same time eliminating evaporation.

In the first series of simulations, sets A to C in Table 1, an OB nanoparticle was placed in the upper vacuum region above the water layer. The simulation was continued for a further 20 ns to allow the OB particle to adsorb on the surface, which is a thermodynamically favored process. An example of the final arrangement of particle and water molecules is shown in Figure 3 for the sulfonate-based OB. Our previous simulations of OB particles in hydrophobic media interacting with water droplets[17] revealed that sulfonate surfactant molecules are capable of detaching from the $CaCO_3$ core (see also refs 33 and 34 for supporting experimental evidence of this trend). This can be attributed to the fact that the charge on the sulfonate headgroup is more distributed than on those of the other surfactant molecules considered in this study.[17] Figure 3 provides further evidence of this effect for the water layer, which can be considered to be a water droplet of effectively infinite radius on the scale of the OB particle. No surfactant dissociation was observed for the SAP and the salicylate-based OB particles seen in Figure 4. The sulfonate-based OB moved fully into and under the water surface because the surfactant dissociation enabled the core to be almost completely covered with water, which is thermodynamically favorable. Figure 4 reveals that, in contrast, the salicylate-based OB sits on the surface of the water, with the surfactant molecules forming a tightly bound stabilizing "crown" around the core on the vacuum side of the interface. Surfactant reorganization around the core on the surface occurred for all surfactant types, which is consistent with conventional hydrophilic−hydrophobic considerations. Control simulations were carried out by rotating the nanoparticle before starting the simulation to confirm that the restructuring of the OB particle on the water surface was independent of the initial orientation of the particle.

After one OB particle had adsorbed on the model water layer and become equilibrated, the layer was extended by 6 nm in the *x*-direction. A second OB particle was then placed in the vacuum layer above this new region, before it was also allowed to adsorb onto the water layer during a further 20 ns of MD simulation. It was found that several attempts of the second particle adsorption had to be made before the second SAP or salicylate OB was able to absorb on the water surface. The use of periodic boundary conditions meant that the second OB particle had less water surface area to adsorb on than the first particle. If the second particle with random initial velocity were initially too close to the OB particle already adsorbed, excluded volume interactions could cause it to move away from the surface before it had time to polarize and structurally modify the water surface in a way which favored adsorption. The second nanoparticle probably needs to polarize the water surface by collective molecule reorientation and reorganization in order for it to be attracted sufficiently strongly to the water surface and to become partly submerged. The propensity for doing this will depend on the instantaneous local structure of the assembly of the water molecules near where the particle approaches the surface.

B. Umbrella Sampling. After the adsorption of the two composite particles a steered MD simulation of 1 ns duration was performed to drive the second OB particle toward the first along the *x*-direction via a nonequilibrium procedure. The calcium and carbonate ions of the first docked particle were restrained with a harmonic potential of 1000 kJ mol^{-1} nm^{-2}. A pulling force of 1000 kJ mol^{-1} nm^{-2} was used, with the pulling rate being 0.01 nm ps^{-1}.[35] The reaction coordinate is the guiding path for the approach of the two nanoparticles. They are initially well separated (>6 nm) and are then bought together by moving one along the reaction coordinate and restraining the other. A global free-energy minimum occurred when the two nanoparticles were in close proximity, yet are still separated by at least one layer of water molecules. A "frame" is a measure of the pulled distance between the two nanoparticles along the *x*-direction. During the steered MD simulation, 1000 frames were generated, which at a pulling rate of 0.01 ns/ps corresponded to a total distance of 10 nm moved in the *x*-direction. Each frame was a starting point for a 500 ps simulation. The 500 frames closest to the PMF minimum (±250) were used to carry out the analysis.

For all surfactant types the pulled particle did not come into direct contact with the other OB particle. Instead, it took an

DOI: 10.1021/acs.langmuir.7b00827
Langmuir 2017, 33, 7263−7270

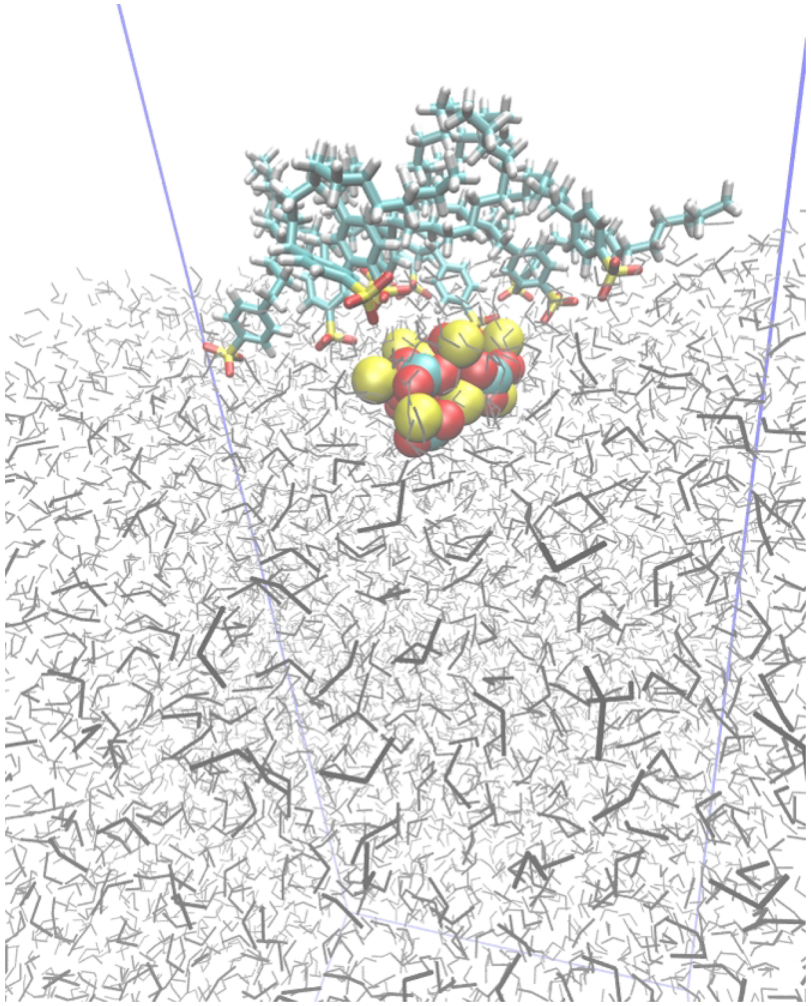


Figure 3. Stabilized sulfonate OB particle at a liquid−vacuum interface. The water molecules are shown in gray. The Ca^{2+} ions are yellow. The carbonate CO_3^{2-} ions are represented by blue and red spheres. The surfactant tails are highlighted in blue.

alternative path around the restrained particle, as shown in Figure 5 for two SAP particles (the *x*-direction is from left to right on the figure). The figure shows the time elapsed trajectory of an OB particle pulled toward the other particle seen in the middle of the figure. The pulled particle can be seen to pass around the other one. The starting point (top left corner) and finishing point (bottom right-hand corner) are indicated in Figure 5. There were always some water molecules between the two particles, even at the point of their closest approach.

Fifty equally spaced snapshots were taken during umbrella sampling across this trajectory, with an extra 10 included near the region where the two particles were in closest proximity. Umbrella sampling was then performed on each of the 60 frames for 10 ns, with the first 2 ns from each window disregarded from the analysis to take account of equilibration at each step.[36] The potentials of mean force (PMFs) were calculated from the trajectories by umbrella sampling using the weighted histogram analysis method (WHAM), *g_wham* procedure,[37] which is optimized for GROMACS. The potential of mean force (PMF) traces for the three different model surfactant-stabilized OB particles are presented in Figure 6. The salicylate has a global minimum of ca. 10 k_BT (44 kJ mol^{-1}), and the SAP and sulfonate cases have values of ca. 8 k_BT (35 kJ mol^{-1}) and 5 k_BT (22 kJ mol^{-1}), respectively. Therefore, the salicylate OB has the most favorable free energy of association, as signified by the deepest free energy well, while the sulfonate particle is the least favorably associated. This result indicates that two sulfonate OB particles would associate less strongly on a water surface than OB particles made from SAP and salicylate surfactants. This is probably due to there being a more tightly bound hydration shell of water molecules around each sulfonate particle which inhibited their close approach because of the associated energy cost of hydration shell restructuring involved. Even though there was always a layer of water between the two particles, the two particles experienced mutual attractive Coulombic and van der Waals interactions. This total energy variation would cause particle clustering of many of them on the surface.

This behavior leads one to conclude that the sulfonate OB component would neutralize ambient acid more rapidly than the other two particle types because the weaker effective pair interaction between the sulfonate particles would lead to them being more spread out over a water droplet surface. This is consistent with the results of experimental studies of the sulfonate OB systems.[33,34,38,39] Apart from the global minimum, the PMF profiles exhibit several local minima at different separations for the three surfactants, which presumably reflect the chemical "architecture" of the particles.

DOI: 10.1021/acs.langmuir.7b00827
Langmuir 2017, 33, 7263−7270

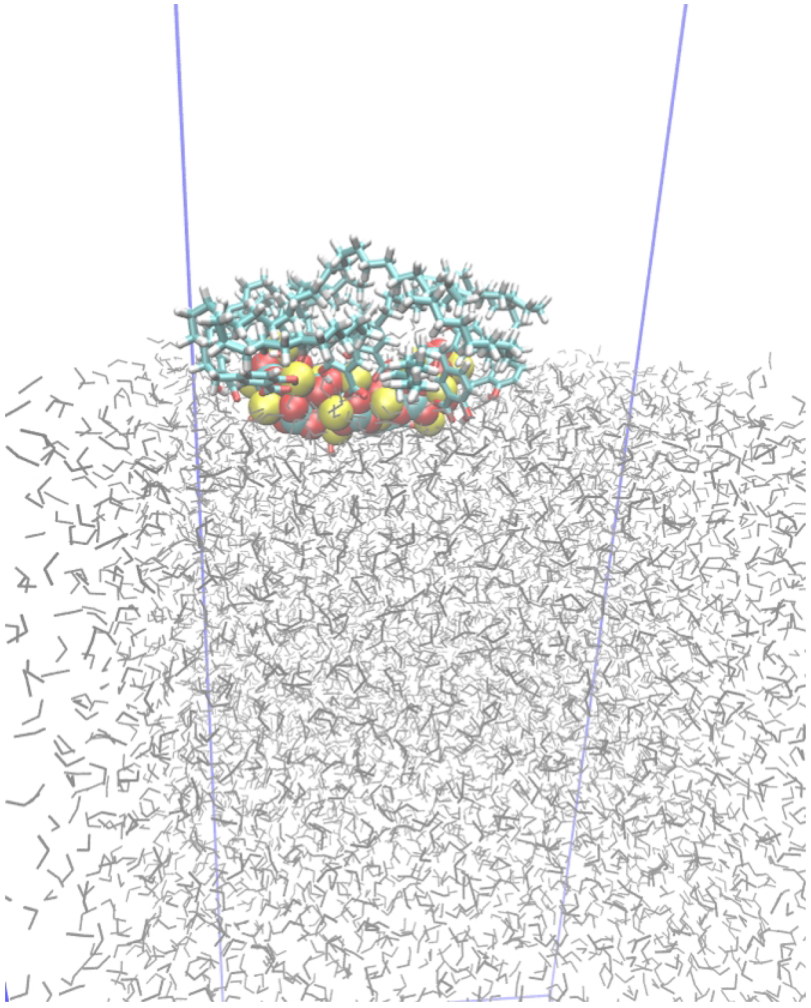


Figure 4. Stabilized salicylate OB particle at the liquid−vacuum interface. The color coding is the same as for Figure 3.

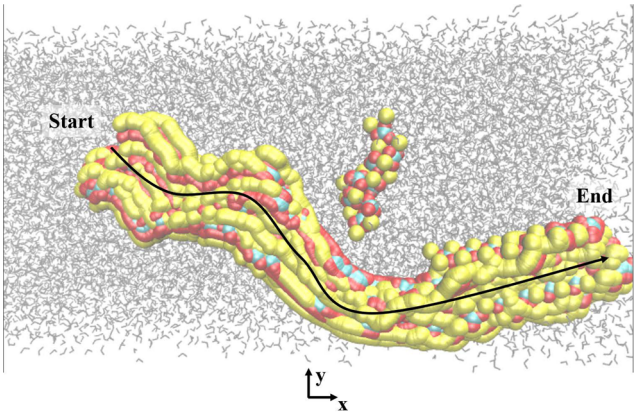


Figure 5. Steered MD trajectory for the SAP-based OB particle. There are two such particles on the surface, with one moving following the trajectory indicated by the black arrow. The ions shown are calcium (yellow) and carbonate (red and blue).

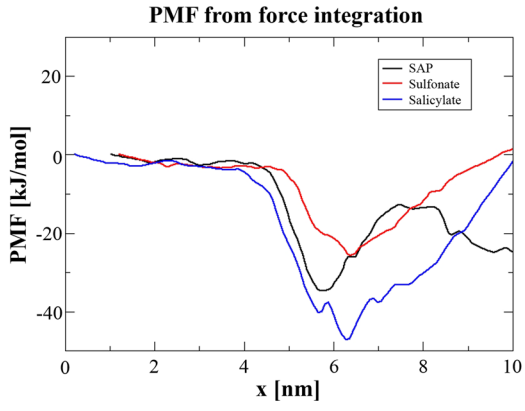


Figure 6. Potential of mean force (PMF) profiles for the three different surfactant-stabilized OB particle types as the two OB particles of the same type are brought together.

In order to gain further insight into the nature of the association of the particles, the intermolecular energies during the steered MD trajectory were examined for each particle type. The majority of the terms in the force field were similar for the three different simulations. However, significant differences were noted in the Coulombic component of the total energy between the restrained particle and the surrounding water molecules. This is plotted for the three OB particle types in Figure 7. The figure shows that the most negative and therefore thermodynamically favorable interactions between the OB particle and hydration shells are for the sulfonate type. The average energy is about twice that of the other two OBs. The dissociation of the sulfonate surfactant molecules from the $CaCO_3$ core and its subsequent immersion below the water−

DOI: 10.1021/acs.langmuir.7b00827
Langmuir 2017, 33, 7263−7270

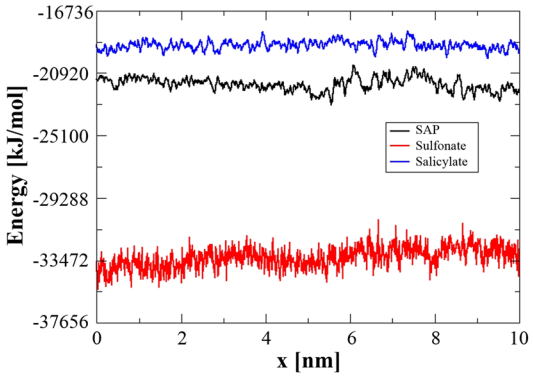


Figure 7. Variation in the solvent−OB Coulombic energy terms throughout the steered MD simulation.

vacuum interface increased the number of "contacts" between the particle and the surrounding water molecules, all factors contributing to the relatively large Coulombic interaction energy between the core and water for the sulfonate type of OB. Because the particle core is essentially covered with water and less protected by the surfactant than the other two types, this behavior could be another factor in causing fast acid neutralization rate found experimentally for sulfonate-based OBs.[33,34,38,39] The acid molecules are in the water.

As the two particles are brought together during the steered MD procedure, the energy terms arising from the SAP and sulfonate surfactants shown in Figure 7 display significant fluctuation, while the salicylate surfactant exhibits a more constant profile. A statistical analysis was performed of the water−water coulomb energy for the 500 frames closest to the free energy minimum shown in Figure 6. The frame numbers used for this analysis ranged between 450 to 950 for SAP, frames 300 to 800 for the sulfonate, and frames 420 to 920 for the salicylate. The same number of frames was used in each case, taking 250 frames either side of the global minimum of the PDF, to obviate any bias. The unpaired Student's *t* test was used to assess the extent to which fluctuations exhibited by each type of OB sample were statistically and therefore dynamically correlated, with the *p*-values given in Table 2. The purpose was

Table 2. Calculated *p*-Values from a Student's *t*-Test Examining the Squared Fluctuation Correlations between Two Different OB Pair Profiles, Using the Solvent−Solvent Coulombic Energy Terms

type of particle	*p*-value
SAP−sulfonate	0.27
SAP−salicylate	<0.0001
sulfonate−salicylate	<0.0001

to investigate the extent to which the fluctuations for two nanoparticles with different surfactants are correlated. Figure 7 shows that the fluctuations in the SAP and sulfonate energies appear to be greater in the 500-frame window than that of the salicylate. The *t* test indicates that the fluctuations for the salicylate NP are significantly different than that of the SAP and sulfonate NP (by the very low *p*-value), suggesting that the underlying dynamical evolution of the salicylate falls into a different category to the SAP and sulfonate cases. The higher the *t* test statistic, *p*, the more likely they are to come from the same distribution and structural evolution process. The *t* test therefore provides further insights into what may simply be drawn by inspection of Figure 7.

The radial distribution function (RDF) between the center of mass of the restrained OB particle and the oxygen atom of a water molecule is shown in Figure 8 for the three particle types.

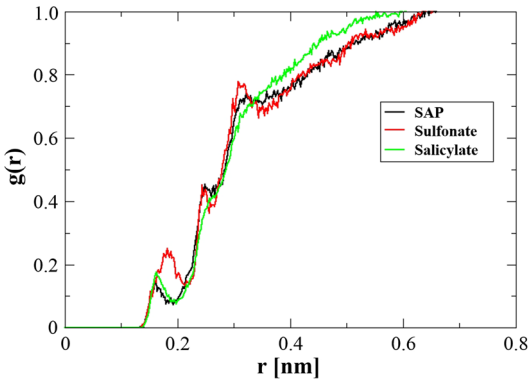


Figure 8. Radial distribution function between the center of mass of the restrained OB and the water oxygen in the simulation.

The figure shows small peaks on a rising background, which are the first, second, and third water coordination shells around the center of mass. In this region the water is mixed with the surfactant headgroups, so these radial "layers" are not entirely composed of water molecules. This figure indicates that the solvent structure around the salicylate particle surface is noticeably different from that around the SAP- and sulfonate-based OBs. All three OBs have a primary peak in their RDF in the range 0.17−0.19 nm. However, only the SAP and sulfonate OBs have secondary and tertiary peaks at 0.24 and 0.30 nm, respectively. The sulfonate-based OB peaks are sharper than those of the SAP and, to a greater extent, the salicylate OBs. This indicates that the water molecules are more ordered around the sulfonate OB, which is consistent with the conclusions based on the PMF profiles. Another reason why the sulfonate RDF is more peaked is that it has the most spherical shaped core,[17] so the shells of water show up more clearly on spherical averaging about the center of mass.

Therefore, to summarize, the increase in solvent ordering could have a significant effect on the value of the free energy PMFs shown in Figure 6. In the process of bringing the two OBs together, it is possible that the more ordered solvent structures around the SAP and sulfonate OB particles have to be disrupted, causing the free energy to increase. The salicylate particle exhibits less long-range solvent ordering, and as the two particles are bought into closer proximity there is a smaller free energy barrier to be overcome, resulting in a more thermodynamically favorable PMF and the most negative free energy of association. It is noteworthy that for all types of nanoparticle there is no *direct* contact as two of them are bought together. The water−water interactions in the hydration shells probably play an equally important role in determining the strength of association between the particles and their effective diameter as the Coulombic and van der Waals terms. These results suggest that the effective diameter of the OB particle obtained from Langmuir trough experiments should be interpreted as including (at least) the first hydration shell around them.

DOI: 10.1021/acs.langmuir.7b00827
Langmuir 2017, 33, 7263−7270

IV. CONCLUSIONS

Figures 3 and 4 reveal that the model overbased detergent particles become structurally quite anisotropic when on a water surface. The hydrophobic tails reorganize on the core surface of the particle to be out of the water surface as much as possible, while the calcium carbonate core is preferentially in contact with the water (in the sulfonate case it is fully immersed below the surface). The particle structure on the surface is not the same as in a bulk hydrophobic solvent, in which it is more spherically symmetric for all surfactant types.

These MD simulations have also shown that the association of two surfactant-stabilized nanoparticles of the same type on a water surface is energetically favorable, with a free energy minimum from the potential of mean force being ca. 5−10 k_BT at typical engine temperatures. The sulfonate particles have a greater affinity for the water surface than the SAP and especially salicylate particles, which may in part explain the relatively rapid rate of acid neutralization found in experiment for this type of particle. Although only simulations with two particles on a water surface have been performed, for computational reasons, they might lead one to conclude that all of the OB particle types should, to varing extents, cluster on a water surface. There is indirect experimental evidence for this, as the experimental overbased particles have been shown to aggregate in the bulk oil.[13] However, the particles appear not to come into direct contact in any of the cases, even at the point of closest approach. There is always a hydration region of water molecules surrounding each particle. The free energy of association between two OB particles is most favorable for the salicylate-based OB and least for the sulfonate case. One possible explanation for this could lie in the water structure around the OB particle and how resistant it is to reorganization as the two particles come together. The simulation results suggest that a salicylate OB particle orders the water molecules less strongly than found for the other types of OB particles considered here. The water structure can adapt to the process when the two particles approach closely, with a smaller energy increase arising from the water−water molecules themselves. The high affinity of the model sulfonate OB particle for water causes this type of particle to associate to the least extent on a water surface. The effective diameter of the OB particle on the water surface is larger than physical size of the particle because of the strongly adhering hydration shell. Previous Langmuir trough experiments may have therefore overestimated the actual size of these particles.

The present simulations show that the association of two species on a water surface can be affected by the extent to which each of them binds to the solvent. This indirectly affects the relative order of the free energy of attraction. A similar trend has been observed for simple Lennard-Jones systems based on protein−ligand complexes.[40−42] This work provides the first example of this effect for this class of inorganic−organic hybrid particle. Although we are concerned here with OB nanoparticle on a flat water surface, these results should also be relevant to OB behavior on the surface of macroscopic water droplets found in an automobile engine, which on the scale of the OB particle dimensions can be considered to be essentially flat. Simulations of the type presented here should become increasingly useful in helping to formulate overbased detergents which satisfy narrowly specified performance requirements.

AUTHOR INFORMATION

Corresponding Author

*E-mail: d.heyes@imperial.ac.uk (D.M.H.).

ORCID

D. Dini: 0000-0002-5518-499X

D. M. Heyes: 0000-0002-4439-4828

Notes

The authors declare no competing financial interest.

ACKNOWLEDGMENTS

M.S.B. thanks BP Pangbourne, UK, for providing him with a Postdoctoral Fellowship which enabled him to carry out this research in the Tribology Group, Department of Mechanical Engineering, Imperial College London. D.D. acknowledges the support received from the EPSRC under the Established Career Fellowship Grant EP/N025954/1. All data can be made available by e-mailing the authors of the paper or tribology@imperial.ac.uk.

REFERENCES

(1) Ottewill, R. H.; Sinagra, E.; MacDonald, I. P.; Marsh, J. F.; Heenan, R. X. Small-angle neutron-scattering studies on nonaqueous dispersions Part 5: Magnesium carbonate dispersions in hydrocarbon media. *Colloid Polym. Sci.* **1992**, *270*, 602−608.

(2) Markovic, I.; Ottewill, R. H.; Cebula, D. J.; Field, I.; Marsh, J. F. Small angle neutron scattering studies on non-aqueous dispersions of calcium carbonate. *Colloid Polym. Sci.* **1984**, *262*, 648−656.

(3) Markovic, I.; Ottewill, R. H. Small angle neutron scattering studies on nonaqueous dispersions of calcium carbonate Part 2. Determination of the form factor for concentric spheres. *Colloid Polym. Sci.* **1986**, *264*, 65−76.

(4) Markovic, I.; Ottewill, R. H. Small angle neutron scattering studies on non-aqueous dispersions of calcium carbonate. Part III. Concentrated dispersions. *Colloid Polym. Sci.* **1986**, *264*, 454−462.

(5) Mansot, J. L.; Hallouis, M.; Martin, J. M. Colloidal antiwear additives 2. Tribological behaviour of colloidal additives in mild wear regime. *Colloids Surf., A* **1993**, *75*, 25−31.

(6) Mansot, J. L.; Wery, J.; Lagarde, P. Local Structure Analysis of the mineral core of reverse micelles in dispersion in Hydrocarbons. *Colloids Surf., A* **1994**, *90*, 167−182.

(7) Cizaire, L.; Martin, J. M.; Le Mogne, T.; Gresser, E. Chemical analysis of overbased calcium sulfonate detergents by coupling XPS, ToF-SIMS, XANES, and EFTEM. *Colloids Surf., A* **2004**, *238*, 151−158.

(8) Martin, J.-M.; Mansot, J. L.; Hallouis, M. Energy filtered electron microscopy (EFEM) of overbased reverse micelles. *Ultramicroscopy* **1989**, *30*, 321−328.

(9) Mansot, J. L.; Hallouis, M.; Martin, J. M. Colloidal antiwear additives 1. Structural study of overbased calcium alkylbenzene sulfonate micelles. *Colloids Surf., A* **1993**, *71*, 123−134.

(10) Tobias, D. J.; Klein, M. L. Molecular Dynamics Simulations of a Calcium Carbonate/Calcium Sulfonate Reverse Micelles. *J. Phys. Chem.* **1996**, *100*, 6637−6648.

(11) Griffiths, J. A.; Bolton, R.; Heyes, D. M.; Clint, J. H.; Taylor, S. E. Physico-chemical Characterisation of Oil-soluble Overbased Phenate Detergents. *J. Chem. Soc., Faraday Trans.* **1995**, *91*, 687−696.

(12) Griffiths, J. A.; Heyes, D. M. Atomistic Simulation of Overbased Detergent Inverse Micelles. *Langmuir* **1996**, *12*, 2418−2424.

(13) Bearchell, C. A.; Edgar, J. A.; Heyes, D. M.; Taylor, S. E. Spectroscopic and Molecular Simulation Evidence for Aggregation of Surfactant-stabilized Calcium Carbonate Nanocolloids in Organic Media. *J. Colloid Interface Sci.* **1999**, *210*, 231−240.

(14) Bearchell, C. A.; Danks, T. N.; Heyes, D. M.; Moreton, D. J.; Taylor, S. E. Experimental and molecular modelling studies of overbased detergent particles. *Phys. Chem. Chem. Phys.* **2000**, *2*, 5197−5207.

DOI: 10.1021/acs.langmuir.7b00827
Langmuir 2017, 33, 7263−7270

(15) Bearchell, C. A.; Heyes, D. M.; Moreton, D. J.; Taylor, S. E. Overbased detergent particles: Experimental and molecular modelling studies. *Phys. Chem. Chem. Phys.* **2001**, *3*, 4774−4783.
(16) Bearchell, C. A.; Heyes, D. M. Molecular Modelling Studies of Calcium Carbonate and its Nanoparticles. *Mol. Simul.* **2002**, *28*, 517−538.
(17) Bodnarchuk, M. S.; Dini, D.; Heyes, D. M.; Chahine, S.; Edwards, S. Self-assembly of calcium carbonate nanoparticles in water and hydrophobic solvents. *J. Phys. Chem. C* **2014**, *118*, 21092−21103.
(18) Bodnarchuk, M. S.; Heyes, D. M.; Breakspear, A.; Chahine, S.; Edwards, S.; Dini, D. Response of Calcium Carbonate Nanoparticles in Hydrophobic Solvent to Pressure, Temperature, and Water. *J. Phys. Chem. C* **2015**, *119*, 16879−16888.
(19) Bodnarchuk, M. S.; Heyes, D. M.; Breakspear, A.; Chahine, S.; Dini, D. A molecular dynamics study of $CaCO_3$ nanoparticles in a hydrophobic solvent with a stearate co-surfactant. *Phys. Chem. Chem. Phys.* **2015**, *17*, 13575−13581.
(20) Clint, J. H.; Taylor, S. E. Particle size and interparticle forces of overbased detergents: A Langmuir trough study. *Colloids Surf.* **1992**, *65*, 61−67.
(21) Mansot, J. L.; Martin, J. B.; Dexpert, H.; Faure, D.; Gallo, R. Local structure analysis in overbased reverse micelles. *Physica B* **1989**, *158*, 237−239.
(22) Courtois, J.-P. Investigation of the Mechanism of Formation of Overbased Detergents. Ph.D. Thesis, University of Surrey, UK, 2002.
(23) Cunningham, I. D.; Courtois, J.-P.; Danks, T. N.; Heyes, D. M.; Moreton, D. J.; Taylor, S. E. Evidence for a fragmentation mechanism during the formation of calcium carbonate organo-nano-particles. *Colloids Surf., A* **2007**, *301*, 184−188.
(24) Parrinello, M.; Rahman, A. Polymorphic transitions in single crystals: A new molecular dynamics method. *J. Appl. Phys.* **1981**, *52*, 7182−7190.
(25) van Der Spoel; Lindahl, D. E.; Hess, B.; Groenhof, G.; Mark, A. C.; Berendsen, H. J. C. GROMACS: fast, flexible, and free. *J. Comput. Chem.* **2005**, *26*, 1701−18.
(26) Pronk, S.; Páll, S.; Schulz, R.; Larsson, P.; Bjelkmar, P.; Apostolov, R.; Shirts, M. R.; Smith, J. C.; Kasson, P. M.; van der Spoel, D.; Hess, B.; Lindahl, E. GROMACS 4.5: a high-throughput and highly parallel open source molecular simulation toolkit. *Bioinformatics* **2013**, *29*, 845−854.
(27) Essmann, U.; Perera, L.; Berkowitz, M. L.; Darden, T.; Lee, H.; Pedersen, L. G. A smooth particle mesh Ewald method. *J. Chem. Phys.* **1995**, *103*, 8577−8593.
(28) Miyamoto, S.; Kollman, P. A. Settle: An analytical version of the SHAKE and RATTLE algorithm for rigid water models. *J. Comput. Chem.* **1992**, *13*, 952−962.
(29) Hess, B.; Bekker, H.; Berendsen, H. J. C.; Fraaije, J. G. E. M. LINCS: A linear constraint solver for molecular simulations. *J. Comput. Chem.* **1997**, *18*, 1463−1472.
(30) Bussi, G.; Donadio, D.; Parrinello, M. Canonical sampling through velocity rescaling. *J. Chem. Phys.* **2007**, *126*, 014101.
(31) Woodcock, L. V. Isothermal molecular dynamics calculations for liquid salts. *Chem. Phys. Lett.* **1971**, *10*, 257−261.
(32) Nosé, S. Constant Temperature Molecular Dynamics Methods. *Prog. Theor. Phys. Suppl.* **1991**, *103*, 1−46.
(33) Fu, J.; Lu, Y.; Campbell, C. B.; Papadopoulos, K. D. Acid Neutralization by Marine Cylinder Lubricants Inside a Heating Capillary: Strong/Weak-Stick Collision Mechanisms. *Ind. Eng. Chem. Res.* **2006**, *45*, 5619−5627.
(34) Fu, J.; Lu, Y.; Campbell, C. B.; Papadopoulos, K. D. Temperature and acid droplet size effects in acid neutralization of marine cylinder lubricants. *Tribol. Lett.* **2006**, *22*, 221−225.
(35) Lemkul, J. A.; Bevan, D. R. Assessing the Stability of Alzheimers Amyloid Protofibrils Using Molecular Dynamics. *J. Phys. Chem. B* **2010**, *114*, 1652−1660.
(36) Torrie, G. M.; Valleau, J. P. Nonphysical sampling distributions in Monte Carlo free-energy estimation: Umbrella sampling. *J. Comput. Phys.* **1977**, *23*, 187−199.
(37) Hub, J. S.; de Groot, B. L.; van der Spoel, D. g_{wham}: A Free Weighted Histogram Analysis Implementation Including Robust Error and Autocorrelation Estimates. *J. Chem. Theory Comput.* **2010**, *6*, 3713−3720.
(38) Totten, G. E.; Shah, R. J. *Fuels and Lubricants Handbook: Technology, Properties, Performance, and Testing*; ASTM International Press: West Conshohocken, 2003.
(39) Rudnick, L. R. *Synthetics, Mineral Oils, and Bio-BasedLubricants: Chemistry and Technology*, 2nd ed.; CRC Press: Boca Raton, FL, 2013.
(40) Baron, R.; Setny, S.; McCammon, J. A. Water in Cavity-Ligand Recognition. *J. Am. Chem. Soc.* **2010**, *132*, 12091−12097.
(41) Setny, P.; Baron, R.; McCammon, J. A. How Can Hydrophobic Association Be Enthalpy Driven? *J. Chem. Theory Comput.* **2010**, *6*, 2866−2871.
(42) Baron, R.; Setny, P.; Paesani, F. Water Structure, Dynamics, and Spectral Signatures: Changes Upon Model Cavity-Ligand Recognition. *J. Phys. Chem. B* **2012**, *116*, 13774−13780.

DOI: 10.1021/acs.langmuir.7b00827
Langmuir 2017, 33, 7263−7270